J Therm Anal Calorim (2017) 127:173–179
DOI 10.1007/s10973-016-5877-9

Thermal analysis on $C_6H_{10}Ge_2O_7$-doped MgB_2

Gheorghe Aldica[1] · Carmen Matei[2] · Adelina Paun[2] · Dan Batalu[2] · Marilena Ferbinteanu[3] · Petre Badica[1]

Received: 29 October 2015 / Accepted: 30 September 2016 / Published online: 14 October 2016

Abstract Additives to MgB_2 can improve the superconducting functional characteristics, such as critical current density (J_c) and irreversibility field (H_{irr}). Recently, we have shown that repagermanium ($C_6H_{10}Ge_2O_7$) is an effective additive, enhancing both J_c and H_{irr}. To look into details of the processes taking place during the reactive sintering, a thermal analysis study (0.167 K s^{-1}, in Ar) is reported. We used differential scanning calorimetry between 298 and 863 K and simultaneous thermogravimetric—differential thermal analysis between 298 and 1233 K. Samples were mixtures of powders with composition 97 mol% MgB_2 and 3 mol% $C_6H_{10}Ge_2O_7$. Up to 863 K, repagermanium decomposes by multiple steps and forms amorphous phases. A reaction with MgB_2 is not observed. Above this temperature, partial decomposition of MgB_2 occurs. Crystalline Ge and MgO are detected before formation of Mg_2Ge and MgB_4, when temperature approaches the melting point of Ge (1211 K). Carbon substitution for boron in the crystal lattice of MgB_2 is observed for samples heated above 863 K. The amount of substitutional C does not significantly change with temperature.

✉ Petre Badica
badica2003@yahoo.com

[1] National Institute of Materials Physics, Atomistilor 405A, 077125 Magurele, Romania

[2] Faculty of Materials Science and Engineering, University POLITEHNICA of Bucharest, Splaiul Independentei 313, 060042 Bucharest, Romania

[3] Inorganic Chemistry Department, University of Bucharest, Dumbrava Rosie 23, 020462 Bucharest, Romania

Keywords MgB_2 · $C_6H_{10}Ge_2O_7$ addition · Thermal analysis · Infrared spectroscopy · X-ray diffraction · Phase transformations

Introduction

MgB_2 is a promising practical superconductor [1], due to its lightness, low price, wide availability, and interesting physics. There are two main routes of obtaining MgB_2 superconducting bulks or powder-in-tube wires/tapes. In the in situ technique, starting materials are pristine Mg and B, while in the ex situ method MgB_2 is used. It was shown that small amounts of different additives can improve functional superconducting characteristics of MgB_2. In practice, higher irreversibility fields, H_{irr}, and critical current densities, J_c, for a constant or a small decrease in the critical temperature, T_c, are required. Additives can produce new MgB_2-based composites or provide substitution elements for B or Mg in the crystal lattice of MgB_2. The as-introduced nano impurities, defects, and local strain-induced lattice deformation may play the role of effective pinning centers for the vortices motion, promoting high J_c. The results strongly depend on the nature of the additives, processing route (in situ or ex situ) and specific features of the technology.

Metalloids (B, Si, Ge, As, Sb, and Te) as pure elements or their compounds have been added to MgB_2 [2]. The most intensively studied are Si-based ones, such as SiC [3–5]. Recently, we have shown that Ge, GeO_2, and $C_6H_{10}Ge_2O_7$ additions to MgB_2 obtained by ex situ spark plasma sintering (SPS) technique significantly enhance the critical current density J_c in high magnetic fields [6–9]. The highest values are obtained for the $C_6H_{10}Ge_2O_7$ additive [6]. This additive has a double action. Namely, it generates

nano impurities of Mg_2Ge and C substitutes B in the crystal lattice of MgB_2 [6]. For further developments, understanding of the processes/reactions taking place during heating/cooling of the $C_6H_{10}Ge_2O_7$–MgB_2 powder mixture is necessary. Thermal analysis is an important investigation tool to reveal the processing transformations of different materials, including superconductors [10–14]. Thermal analysis was applied on mixtures of Mg and B (Mg_xB_2, $x = 0.1$, 0.5, 1.0, 1.5, 3.0) in Refs. [12–14] to observe different stages of MgB_2 phase formation. Thermal analysis studies were also used to investigate Fe-sheathed ex situ powder-in-tube MgB_2 tapes after mechanical deformation and vacuum annealing processes [15].

The bis-carboxyethyl germanium sesquioxide ($C_6H_{10}Ge_2O_7$), also known as repagermanium (RGe), carboxyethylgermanium, or Ge-132, was synthesized in 1967 and structurally characterized in 1976 [16]. It has been intensively studied especially as a dietary supplement [17, 18], anticancer active substance [19–21], and as a useful substance for other medical applications [22]. It was proved to have a very low toxicity [23, 24].

To understand the reactive sintering processes of added MgB_2, we report the thermal behavior of the MgB_2–$C_6H_{10}Ge_2O_7$ mixture. We used differential scanning calorimetry (DSC), thermogravimetric analysis (TG), and complementary measurements at room temperature of X-ray diffraction (XRD) and Fourier transform infrared spectroscopy (FTIR) on specimens heated at different temperatures.

Experimental

MgB_2 (Alfa Aesar, 99.5 % purity) and $C_6H_{10}Ge_2O_7$ (Alfa Aesar, 99.7 % purity) commercial powders were mixed with composition $(MgB_2)_{0.97} + (C_6H_{10}Ge_2O_7)_{0.03}$.

For thermal analysis measurements, we used a Netzsch DSC 204 F1 apparatus (Al crucible), between 298 and 863 K, and a SETARAM Setsys Evolution 18 thermogravimeter (Al_2O_3 crucible) in TG–DTA mode, between 298 and 1233 K. The experiments were conducted in argon, at a flow rate of 3.3×10^{-7} m^3 s^{-1}. The heating rate was of 0.167 K s^{-1}. The mass of the samples in the thermal analysis experiments is indicated in Tables 1 and 2. Sample notation indicates the maximum temperature attained in the thermal analysis experiments.

The X-ray diffraction technique (XRD, Bruker-AXS D8 ADVANCE, $Cu_{K\alpha 1}$ radiation, $\lambda = 1.54056$ Å) was performed at room temperature on samples heated at different temperatures.

A JASCO 4200 spectrometer was used to measure Fourier-transformed infrared (FTIR) spectra in the range 400–4000 cm^{-1}. Samples were prepared using KBr. As in the case of XRD, measurements were done at room temperature on samples heated at 493, 593, 643, 710, 783, 863, 973, 1043, 1088, 1143, and 1233 K.

Results and discussion

Thermal analysis from room temperature to 863 K

In the 398–863 K temperature range, added MgB_2 shows specific thermal transformations for $C_6H_{10}Ge_2O_7$ (Fig. 1). Differences are rather small, and this suggests that reactions at these temperatures between $C_6H_{10}Ge_2O_7$ and MgB_2 are limited or lacking. Seven transformations (Table 1) are observed, and they correspond to different stages of $C_6H_{10}Ge_2O_7$ transformations.

The first transformation at ~465 K (I, Fig. 1) and at 445 K in the heating and cooling regimes, respectively, was ascribed to a reversible isomerization of $C_6H_{10}Ge_2O_7$. Details are presented elsewhere [25]. The reversibility of this transformation cannot be easily visualized in the cooling regime (Fig. 1b) due to the low amount of $C_6H_{10}Ge_2O_7$ in the mixture and disperse character. Phase assembly (Fig. 2) and bonds (Fig. 3) observed at room temperature by XRD and FTIR before and after thermal analysis (samples 'RT' and '493') are similar, and hence, they support the idea of an isomerization transformation.

Transformations denoted II–VII (Fig. 1) are irreversible, and this suggests the decomposition of $C_6H_{10}Ge_2O_7$. Transformations II–VII are accompanied by mass loss [25], meaning that decomposition of organics occurs. Processes and possible decomposition scenarios are discussed in [25]. Noteworthy, is that transformations are better revealed in this work than in [25]. Namely, this is especially the case for transformations V–VII at 707, 755, and 789 K. Due to this, the shape of the thermal analysis curves and positions of the peaks are not identical between the two works. A reason for the encountered differences is that the presence of MgB_2, although it does not react with $C_6H_{10}Ge_2O_7$ and keeps its phase integrity with temperature, can favor the release of resulted gases from the ($MgB_2 + C_6H_{10}Ge_2O_7$) mixture, and through this, can influence the heat transfer behavior of the sample.

A special remark is related to transformation II taking place at 545 K on heating (Fig. 1a) and at ~533–543 K on cooling (Fig. 1b) for samples ('493,' '593,' '643,' '710,' and '863') heated above 493 K, but below 863 K. The two peaks on heating and on cooling are not necessarily reflecting the same transformation. In Table 1, for each sample, we indicate the temperatures of the beginning and of the end of this transformation. These temperatures were determined by applying a tangent to the DSC cooling curves. There is a broadening of the peak at ~543 K on

Table 1 Samples, samples mass, thermal effects, and decomposition moieties/residuals

Sample/mass/10^{-6} kg	Heating stage Temperature/K	DSC event heating/cooling		Thermal effect on heating/cooling/K	Lost chemical fragment of $C_6H_{10}Ge_2O_7$ or phase formation
		T_{onset}/K	T_{offset}/K		
'493'/21.65	I/298–493	438/454	484/414	Endothermic 464/ Exothermic 444	Reversible effect
'593'/13.13	II + III/493–593	II: 488/573	560/468	Endothermic 545/	Hydroxylic groups
		III: ~570/–	588/–	Exothermic 533	
				Exothermic 576/–	
'643'/14.32	IV/593–643	615/598	646/449	Exothermic 633/ Exothermic 536	Alkyl fragments
'710'/15.22	V/643–723	687/619	723/438	Exothermic 703/ Exothermic 540	Alkyl fragments
'783'/17.49	VI/723–783	741/635	771/427	Exothermic 755/ Exothermic 541	Hydroxylic groups
'863'/11.57	VII/783–863	788/655	792/423	Endothermic 789/ Exothermic 543	Amorphous Ge + C + O

Table 2 Samples, samples mass, thermal effects, and phase formation

Sample/mass/10^{-6} kg	Heating stage Temperature/K	DSC event heating/cooling		Thermal effect on heating/cooling/K	Phase formation
		T_{onset}/K	T_{offset}/K		
'863'/11.57	VII/783–863	788/655	792/423	Endothermic 789/ Exothermic 543	Amorphous Ge + C + O
'973'/26.22	VIII + IX/855–965	VIII: 855/–	908/–	Exothermic, ~873/–	Ge crystalline (cr.), some Mg gas
		IX: 917/–	957/–	Exothermic, ~933/–	
'1043'/21.74	X + XI/965–1033	X: 960/–	982/–	Exothermic, ~968/–	More Ge cr., MgO
		XI: 977/–	1018/–	Exothermic, 1004/–	
'1088'/19.31	XII/1033–1088	1028/–	1061/–	Exothermic, ~1047/–	Max. Ge cr., more MgO
'1143'/30.26	XIII/1088–1143	1103/–	1133/–	Endothermic, 1118/–	Low Ge cr., more MgO, Mg_2Ge
'1223'/19.37	XIV/1143–1233	1213/–	>1233/–	Exothermic, >1233/–	Traces of Ge cr., max. MgO, Mg_2Ge, MgB_4

cooling, while its maximum slightly increases when samples are heated to higher temperatures. This behavior is observed also for the individual $C_6H_{10}Ge_2O_7$ powder decomposition [25], and it suggests that it is due to a certain rearrangement during cooling although $C_6H_{10}Ge_2O_7$ significantly changes its identity. While MgB_2 is not directly involved, it is worth mentioning that Mg, detected by XRD in our samples 'RT' (raw powder mixture not heated) '493,' '593,' '643,' '710,' and '863,' has a melting temperature of 923 K, and a eutectic between Mg and C forms at 688 K [26]. In the samples heated up to higher temperatures than 863 K, Mg cannot be observed in the XRD patterns (Fig. 2), and the peak on cooling at ~543 K vanishes. Further investigations are required to clarify the observed behavior.

FTIR spectra have different patterns for different samples (Fig. 3). Sample 'RT' shows the characteristic bands of $C_6H_{10}Ge_2O_7$ and of MgB_2. Several bands with low intensities that are observed in the 480–540 and 650–700 cm^{-1} region are attributed to MgB_2 [27]. Carboxylic groups are represented by a strong band at 1710–1780 cm^{-1} assigned to a stretching $\nu_{C=O}$ bond, and by a broad band at 2500–3000 cm^{-1} due to the stretching ν_{O-H} bond. The organic skeleton is represented by several weak and medium absorption bands associated with ν_{C-H} in CH_2—1460 cm^{-1} and ν_{C-C} 1200–700 cm^{-1} frequency modes. Bands between 550 and 850 cm^{-1} in the spectra of the 'RT' sample correspond to O–Ge–O stretching and deformation modes [28–31] of the fragments originating from $C_6H_{10}Ge_2O_7$.

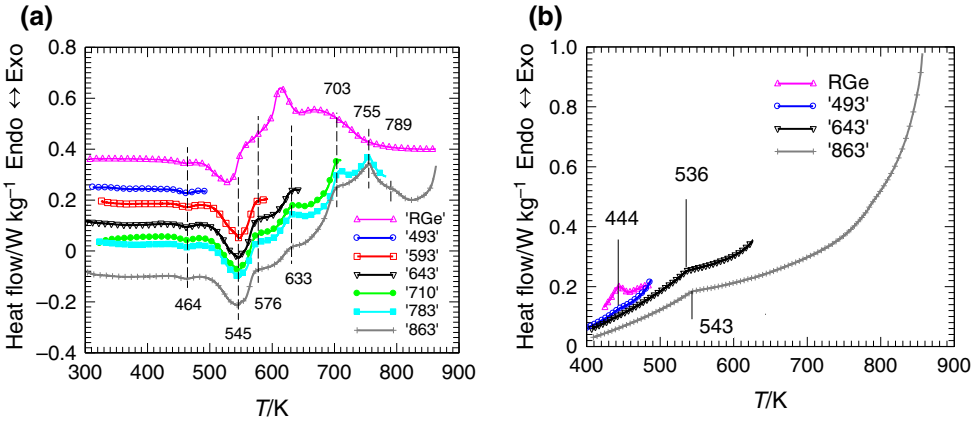

Fig. 1 **a** Thermodynamic transitions for samples from the MgB_2 and $C_6H_{10}Ge_2O_7$ mixture between 298 and 863 K (0.167 K s^{-1}, heating) and for pristine $C_6H_{10}Ge_2O_7$ (sample 'RGe'); **b** Thermodynamic transitions of some selected samples between 393 and 863 K (0.167 K s^{-1}, cooling)

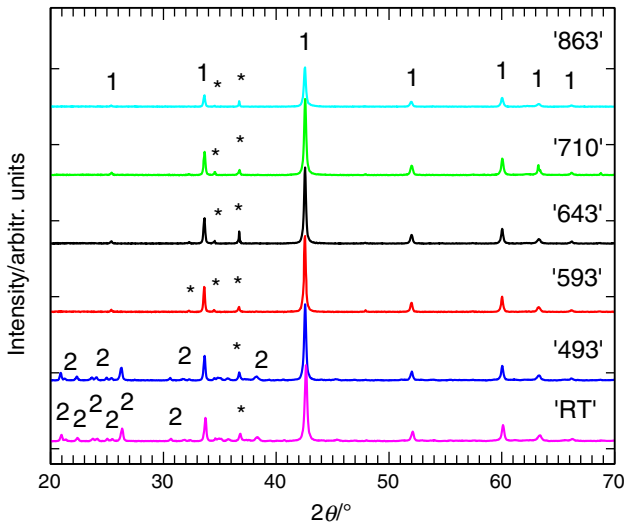

Fig. 2 XRD patterns of the raw powder mixture ('RT') and for the samples cooled down from different heating temperatures. Phase notation: 1-MgB_2, 2-$C_6H_{10}Ge_2O_7$, and *-Mg

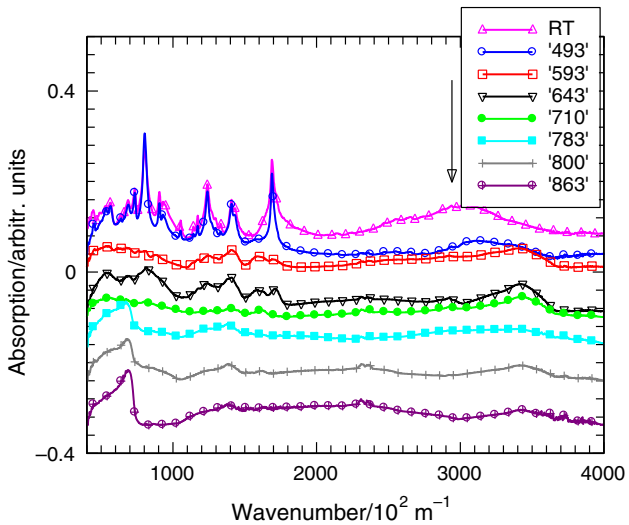

Fig. 3 FTIR spectra for the raw mixture (RT) and for the samples cooled down from different heating temperatures. *Arrow* indicates the increase in the heating temperature

Thermal analysis experiments between 863 and 1233 K

In the range of temperature 863–1233 K, TG-DSC apparatus recorded the formation of relatively stable and metastable (Ge) crystalline phases. Seven transformations were identified by DSC analysis (Fig. 4; Table 2). Transformations VIII–XII and XIV are exothermic, while the XIII is endothermic. On cooling, thermal effects were addressed in Sect. 3.1.

XRD indicates on occurrence of the crystalline Ge-metal between 973 and 1143 K and of MgO above 973 K (Fig. 5). At higher temperatures, above 1143 K, Mg_2Ge and MgB_4 phases are observed.

The FTIR spectrum (Fig. 6) shows intensive and overlapped bands at 400–800 cm^{-1}. These bands are the characteristic ones of MgB_2 [27], MgO [32, 33], and Mg_2Ge [34]. In the absence of reported IR spectral data for MgB_4 [35–38], we performed a simple density functional theory (DFT) simulation and estimated that in the same wave-number-region, bands with small intensities of MgB_4 are available. Additional bands at higher wavenumbers can be observed, and they are associated partially with the chemical bonds of adhered contaminants (mainly water and carbon) on the surface of the samples and to the newly formed phases. Bands ν_{O-H} (stretching)-(hydrogen bonded) of the hydroxyl group and C–H are located at 2900–3500 cm^{-1}, H–B terminal bonds at 2300–2400 cm^{-1}, C=C vibration in stretching mode at 1460–1600 cm^{-1}, B–C vibration at 1350–1450 cm^{-1} [39].

Samples show variation of *a* lattice parameter of MgB_2 phase, while the *c* lattice parameter is approximately constant. This is the typical signature of carbon substitution for boron in the crystal lattice of MgB_2 [40, 41]. Namely, for the raw MgB_2 powder and samples heated up to 863 K, the values of *a* can be considered constant at 3.086 Å, while

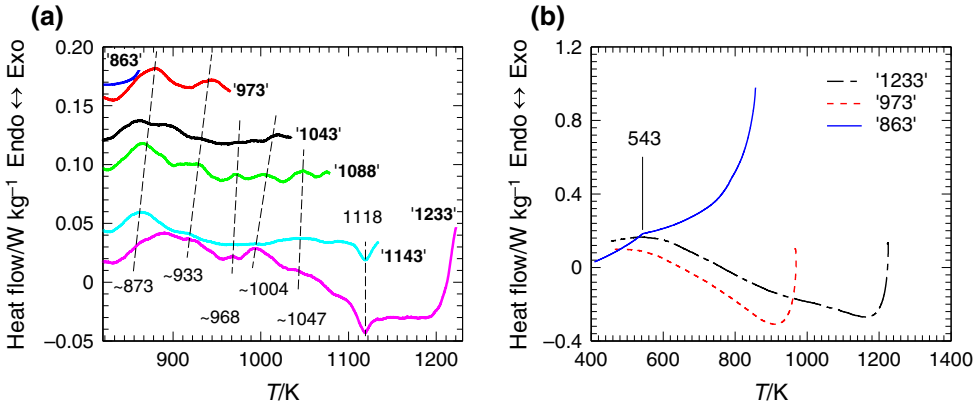

Fig. 4 **a** Thermodynamic transitions in heating regime (0.167 K s^{-1}) for samples heated up to 1233 K. **b** Similar curves in cooling regime (0.167 K s^{-1}) for selected samples

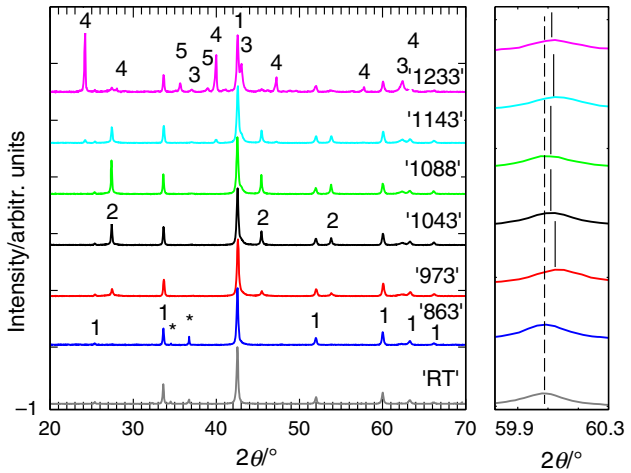

Fig. 5 XRD patterns of samples, cooled down from different temperatures. Phase notation: 1-MgB_2, 2-Ge, 3-MgO, 4-Mg_2Ge, 5-MgB_4, and *-Mg. In the right panel, one observes the shift (when $T > 863$ K) to higher 2θ of the (110) peak due to carbon substitution for boron in the crystal lattice of MgB_2

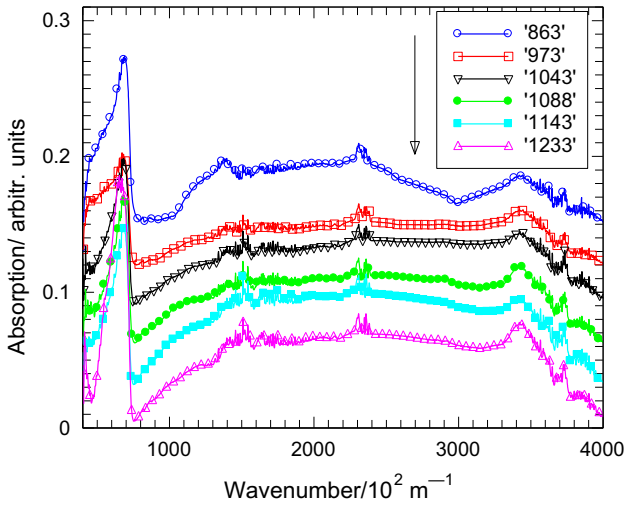

Fig. 6 FTIR spectra for samples cooled down from different heating temperatures. *Arrow* indicates the increase in the heating temperature

for the samples heated at 973 K and at higher temperatures, the values of a are lower, taking values around 3.082 Å. Considering the literature [40, 41] and our data, this corresponds to an enhancement of the amount of carbon (x) for the chemical formula $Mg(B_{1-x}C_x)_2$ from 0.003 to 0.011 (error is ±0.0005). In summary, substitution of boron by carbon takes place at 863–973 K (Fig. 5). As already noted, at these temperatures, the decomposition and removal of the organic part of $C_6H_{10}Ge_2O_7$ ends up. Although samples show some scattering of x—carbon, at higher temperatures, substitution processes does not show a significant development since no source of carbon remains in the mixture. This information is useful technologically because it provides the background for a relatively independent control of the carbon substitution and of the secondary nanophases formation, both aspects being well known to influence the flux pinning in MgB_2-based superconducting materials.

In order to orient ourselves in the assignment of vibration spectra, in relation to the structural changes in MgB_2, routine electron structure calculations [42] were performed on simplified models. Thought very crude, we considered molecular $\{B_6\}$ and $\{B_5C\}$ rings, in the form of $B_6H_6^{2-}$ and $B_5CH_6^-$ species. The double negative charge on the boron ring resolves the electron deficiency of boron, filling the total symmetric π-type molecular orbital, in a manner comparable to the charge transfer established between magnesium sites and boron sheets in the band structure of the solid MgB_2. The single negative charge on the carbon-substituted system keeps the isoelectronic configuration. The calculations were done in the frame of density functional theory, using the B3LYP functional and the 6-311G* basic set. The geometry optimization gives a hint about the bond lengths overall scheme. Taking as approximate measure the perimeter of the rings, the modeling shows a relative shrinkage of 2.75 % in the $\{B_5C\}$ system, comparatively to the $\{B_6\}$, in line with the information from XRD. The calculation of vibration spectra on the optimized

$B_6H_6^{2-}$ molecular model shows that B–B frequencies occur at about 364, 648, 674, 705, 843, 848, and 1151 cm^{-1}. However, not all these frequencies are getting IR intensity, in this calculated spectrum being visible the 705 cm^{-1} value due to asymmetric ring deformation. The B–H frequencies occur at 2190 cm^{-1}. The $B_5CH_6^-$ system has lower symmetry, having as consequence the intensity gain in more collective ring vibrations, due to B–B and B–C bonds. The B–B and B–C frequencies occur with low intensities at 660, 717, 770, 910, 1229, and 1376 cm^{-1} and B–H and C–H with higher intensities at 2393–2457 and 2957 cm^{-1}, respectively. By extrapolating the molecular modeling results and comparing with the experimental spectra, one may obtain hints for the comparison of the carbon-doped phase with the pristine MgB_2 lattice. The presence of the bands B–C (1350–1450 cm^{-1}) can be illustrative in this sense.

Conclusions

Thermodynamic transformations during heating and cooling of a mixture with composition 97 mol% MgB_2 and 3 mol% $C_6H_{10}Ge_2O_7$ were revealed. From room temperature up to 863 K, there are multiple steps of $C_6H_{10}Ge_2O_7$ transformations mainly of decomposition and evaporation of the organic part without any clear interaction with MgB_2. At 863–973 K, the process of carbon substitution for boron in the crystal lattice of MgB_2 occurs. In the temperature range of 863–1233 K are observed a partial decomposition of MgB_2, the presence of crystalline Ge and MgO, and formation of Mg_2Ge and MgB_4 phases before Ge-melting at 1211 K.

Acknowledgements This work was performed within Partnership program in the priority domains—PN II, funded by MEN-UEFISCDI, project No. 214/2014 BENZISUPRA. Authors acknowledge Dr. V. Mihalache for XRD measurements and Dr. I. Pasuk for useful discussions.

References

1. Nagamatsu J, Nakagawa N, Muranaka T, Zenitani Y, Akimitsu J. Superconductivity at 39 K in magnesium diboride. Nature. 2001;410:63–4.
2. Batalu D, Aldica G, Burdusel M, Badica P. Short review on rare earth and metalloid oxide additions to MgB_2 as a candidate superconducting material for medical applications. Key Eng Mater. 2015;638:357–62.
3. Cimberle MR, Novak M, Manfrinetti P, Palenzona A. Magnetic characterization of sintered MgB_2 samples: effect of substitution or 'doping' with Li, Al and Si. Supercond Sci Technol. 2002;15:43–7.
4. Dou SX, Soltanian S, Horvat J, Wang XL, Zhou SH, Ionescu M, Liu HK, Munroe P, Tomsic M. Enhancement of the critical current density and flux pinning of MgB_2 superconductor by nanoparticle SiC doping. Appl Phys Lett. 2002;81:3419–21.
5. Yeoh WK, Dou SX. Enhancement of H_{c2} and J_c by carbon-based chemical doping. Phys C. 2007;456:170–9.
6. Batalu D, Aldica G, Popa S, Miu L, Enculescu M, Negrea RF, Pasuk I, Badica P. High magnetic field enhancement of the critical current density by Ge, GeO_2 and $Ge_2C_6H_{10}O_7$ additions to MgB_2. Scr Mater. 2014;82:61–4.
7. Batalu D, Aldica G, Burdusel M, Popa S, Enculescu M, Pasuk I, Miu D, Badica P. Ge-added MgB_2 superconductor obtained by ex situ spark plasma sintering. J Supercond Nov Magn. 2015;28:531–4.
8. Batalu D, Aldica G, Popa S, Kuncser A, Mihalache V, Badica P. GeO_2-added MgB_2 superconductor obtained by spark plasma sintering. Sol State Sci. 2015;48:23–30.
9. Batalu D, Aldica G, Badica P. $Ge_2C_6H_{10}O_7$-added MgB_2 superconductor obtained by ex situ spark plasma sintering. IEEE Trans Appl Supercond. 2016;26:7100104.
10. Ozturk O, Gokcen T, Cavdar S, Koralay H, Tasci AT. A study on nucleation, crystallization kinetics, microstructure and mechanical properties of Ru–Bi partial substituted BSCCO glass ceramics. J Therm Anal Calorim. 2016;123:1073–82.
11. Matskevich NI, Minenkov YF, Berezovskii GA. Calorimetric study and stability of Y2O2 phase in the Y–Ba–Cu–O system. J Therm Anal Calorim. 2015;121:771–6.
12. Kang DK, Kim DW, Choi SH, Kim CA, Ahn IS. Phase formation of MgB_2 superconducting materials fabricated by spark plasma sintering. Metal Mater Int. 2009;15(1):15–9.
13. Yan SC, Yan G, Liu CF, Lu YF, Zhou L. Experimental study on the phase formation for the Mg–B system in Ar atmosphere. J Alloys Compd. 2007;437:298–301.
14. Ma ZQ, Liu YC. Low-temperature synthesis of MgB_2 superconductors. Inter Mater Rev. 2011;56:267–86.
15. Lezza P, Gladyshevskii R, Suo HL, Flukiger R. Quantitative study of the inhomogeneous distribution of phases in Fe-sheathed ex situ MgB_2 tapes. Supercond Sci Technol. 2005;18(5):753–7.
16. Tsutsui M, Kakimoto N, Axtell DD, Oikawa H, Asai K. Crystal-structure of carboxyethylgermanium sesquioxide. J Am Chem Soc. 1976;98(25):8287–9.
17. Kaplan BJ, Parish WW, Andrus GM, Simpson JSA, Field CJ. Germane facts about germanium sesquioxide: I. Chemistry and anticancer properties. J Altern Complem Med. 2004;10:337–44.
18. Jirasko R, Holcapek M, Rosenberg E. Characterization of bis-carboxyethyl germanium sesquioxide and its complexes with amino acids using electrospray QqTOF mass spectrometry. Inter J Mass Spectrom. 2009;280:198–203.
19. Shangguan GQ, Huang LL, Qu XG. The synthesis and cytotoxic activity of novel organogermanium sesquioxides with anthraquinone or naphthalene moiety. Chin Chem Lett. 2007;18:1347–50.
20. Shangguan G, Xing F, Qu X, Mao J, Zhao D, Zhao X, Ren J. DNA binding specificity and cytotoxicity of novel antitumor agent Ge132 derivatives. Bioorg Med Chem Lett. 2005;15:2962–5.
21. Pi J, Zeng J, Luo JJ, Yang PH, Cai JY. Synthesis and biological evaluation of germanium(IV)–polyphenol complexes as potential anti-cancer agents. Bioorg Med Chem Lett. 2013;23:2902–8.
22. Nakamura T, Nagura T, Akiba M, Sato K, Tokuji Y, Ohnishi M, Osada K. Promotive effects of the dietary organic germanium poly-trans-[(2-carboxyethyl) germasesquioxane] (Ge-132) on the secretion and antioxidative activity of bile rodents. J Health Sci. 2010;56:72–80.
23. Shimada Y, Sato K, Tokuji Y, Nakamura T. Nuclear magnetic resonance studies of the interactions between the organic germanium compound Ge-132 and saccharides. Carbohyd Sci. 2015;407:10–5.

24. Nakamura T, Saito M, Shimada Y, Fukaya H, Shida Y, Tokuji Y. Induction of aminolevulinic acid synthase gene expression and enhancement of metabolite, protoporphyrin IX, excretion by organic germanium. Eur J Pharmacol. 2011;653:75–81.
25. Batalu D, Paun A, Ferbinteanu M, Aldica G, Badica P. Thermal analysis of repagermanium. Themochim Acta. doi:10.1016/j.tca.2016.10.005.
26. Hu B, Du Y, Xu H, Sun W, Zhang WW, Zhao D. Thermodynamic description of the C-Ge and C-Mg systems. J Min Metall Sect B Metall. 2010;46:97–103.
27. Alarco JA, Chou A, Talbotab PC, Mackinno IDR. Phonon modes of MgB_2: super-lattice structures and spectral response. Phys Chem Chem Phys. 2014;16:24443–56.
28. Galeener FL, Leadbetter AJ, Stringfellow MW. Comparison of the neutron, Raman, and infrared vibrational spectra of vitreous SiO_2, GeO_2, and BeF_2. Phys Rev B. 1983;27:1052–78.
29. Rivillon S, Chabal YJ, Amy F, Kahn A. Hydrogen passivation of germanium (100) surface using wet chemical preparation. Appl Phys Lett. 2005;87:253101.
30. Salvi TBD, Job EA, Ribeiro JLS. New flexible and transparent solution-based germanium-sulfide polymeric materials. J Braz Chem Soc. 2015;26:992–1003.
31. Lee GE, Seto YJ, Hirao T, Bernath FP, LeRoy JR. FTIR emission spectra, molecular constants, and potential curve of ground state GeO. J Mol Spectr. 1999;194:197–202.
32. Hanna R. Infrared properties of magnesium oxide. J Am Ceram Soc. 1965;48(7):376–80.
33. Adebayo GA, Liang Y, Miranda CR, Scandolo S. Infrared absorption of MgO at high pressures and temperatures: a molecular dynamic study. J Chem Phys. 2009;131:014506.
34. Lott LA, Lynch DW. Infrared absorption in Mg_2Ge. Phys Rev. 1966;141(2):681–6.
35. Nyquist RA, Kagel RO. Infrared Spectra of Inorganic Compounds (3800–45 cm^{-1}), vol. 4. San Diego: Academic Press; 1971.
36. Gogotsi YG, Andrievski RA, editors. Material science of carbide, nitride and borides. Berlin: Kluwer Academic Publishers; 1999.
37. Brame EG Jr, Margrave JL, Meloche VW. Infra-red spectra of inorganic solids—II oxides, nitrides, carbides, and borides. J Inorg Nucl Chem. 1957;5(1):48–52.
38. Yang GR, Zhao YP, Tong BY. FTIR and uv study of amorphous silicon-boron alloys deposited by LPCVD. MRS Proc. 1996;426:83. doi:10.1557/PROC-426-83.
39. Paskevicius M, Pitt MP, Webb CJ, Sheppard DA, Filso U, Gray EM, Buckley CE. In-situ x-ray diffraction study of gamma-$Mg(BH_4)(2)$ decomposition. J Phys Chem C. 2012;116:15231–40.
40. Dou SX, Shcherbakova O, Yeoh WK, Kim JH, Soltanian S, Wang XL, Senatore C, Flukiger R, Dhalle M, Husnjak O, Babic E. Mechanism of enhancement in electromagnetic properties of MgB_2 by nano SiC doping. Phys Rev Lett. 2007;98:097002.
41. Lee S, Masui T, Yamamoto A, Uchiyama H, Tajima S. Crystal growth of C-doped MgB_2 superconductors: accidental doping and inhomogeneity. Phys C. 2004;412–414:31–5.
42. Frisch MJ, et al., editors. Gaussian 03, revision B.04. Pittsburgh: Gaussian, Inc.; 2003.